Journal of Sound and Vibration 329 (2010) 3082–3100

Contents lists available at ScienceDirect

Journal of Sound and Vibration

journal homepage: www.elsevier.com/locate/jsvi

Sound transmission through a double panel structure periodically coupled with vibration insulators

Julien Legault *, Noureddine Atalla

GAUS, Department of Mechanical Engineering, Univ. de Sherbrooke, Sherbrooke, Quebec, Canada J1K 2R1

ARTICLE INFO

Article history:
Received 19 August 2009
Received in revised form
4 February 2010
Accepted 10 February 2010
Handling Editor: M.P. Cartmell
Available online 11 March 2010

ABSTRACT

In this paper, sound transmission through an aircraft sidewall representative double panel structure is investigated theoretically and parametric and validation studies are conducted. The studied configuration is composed of a trim panel (receiver side panel) attached to a ribbed skin panel (source side panel) with periodically spaced resilient mounts. The structure is considered infinite in order to use space harmonic expansion. The partition is also assumed planar for simplicity. The model allows for a 3D incident field and the panels can be metallic and/or composite. A four-pole formulation is employed for modeling of the mounts and the absorption provided by the fiberglass that fills the cavity between the leaves is addressed with an equivalent fluid model. The investigation of mount stiffness, damping and spacing show that properly designed mounts can increase the TL significantly (up to 20 dB of difference between rigid and resilient mounts). However, they can create undesirable resonances resulting from their interaction with the panels. The influence of cavity absorption is also studied and results illustrate the fact that it is not worth investing in a highly absorbent fiber if the structure-borne transmission path is not adequately insulated, and likewise that it is not worth investing in highly resilient mounts without sufficient cavity absorption. Moreover, the investigation of panel damping confirms that when structure-borne transmission is present, raising skin damping can increase the TL even below coincidence, but that on average, greater improvements are achieved by raising trim damping. Finally, comparison between the periodic model and finite element simulations for structure-borne transmission shows that the average level of transmitted energy is well reproduced with the periodic approach. However, the modes are only captured approximately due to the assumption of an infinite structure.

1. Introduction

The transmission loss through composite panels has been largely studied over the years. For instance, Koval studied sound transmission through an infinite laminated composite cylindrical shell excited by an oblique plane wave [1]. His work was revisited by Blaise and Lesueur [2] who later proposed a model for diffuse field transmission into 2D [3] and 3D [4] multi-layered infinite cylinders. More recently, Heron [5] and Ghinet et al. [6,7] addressed the problem of sound transmission through laminates and sandwich composite panels using a discrete layer formulation.

However, as reported by Yin et al. [8], less attention has been paid to the sound radiation and transmission of these types of structures when they are periodically stiffened or when they are periodically linked to a companion structure,

* Corresponding author. Tel.: +1 819 821 8000x62122.
E-mail address: julien.legault@usherbrooke.ca (J. Legault).

0022-460X/$ - see front matter © 2010 Elsevier Ltd. All rights reserved.
doi:10.1016/j.jsv.2010.02.013

even though stiffening or linking are present in many practical situations [9,10]. This is particularly true in the case of airplane cabins because the trim, i.e. the receiver side panel, is mounted on periodically spaced ring frames that are ribbed to the skin (source side panel). Moreover, the mounts attaching the trim to those rings are usually resilient and a sound treatment package is inserted in the cavity between the panels. Traditionally, the skin was composed of an aluminum panel stiffened by stringers and ring frames, but composite panels are currently replacing this design due to their excellent stiffness to weight ratio and resistance to fatigue. Unfortunately, these panels depict poorer acoustic performance: predictions and measurements [11] both show that their transmission loss is generally inferior or at best equal to their mass law contour. For this reason, designing efficient noise control systems for composite structures is essential and modeling tools must therefore be provided to assist engineers in this task.

To the authors' knowledge, a simplified analytical model assessing sound transmission through a structure having all the aforementioned features has not been presented in the literature. FEM and FEM-BEM based models are classically used to address this problem, but the good precision they generally provide comes with a high cost of calculation. The objective here is to derive a simple approach that will certainly be limited in complexity, yet suitable for quick parameter studies and optimization and thus useful at early design stages. To respect this constraint, several simplifications are necessary. First, the double wall partition is considered infinite, which allows the dynamics of its sub-systems to be formulated using Mead and Pujara's space harmonics technique [12]. The structure is also assumed flat for purposes of simplicity and because accounting for a cylindrical structure requires usage of combined space harmonic/modal displacement fields [13] that would render calculations exceedingly onerous. This limitation is however acceptable since the effect of curvature is mainly important around and below the ring frequency and this usually happens at low frequencies (e.g. below 450 Hz for an aluminum fuselage with a radius of curvature of 2 m) where the presented model is questionable anyhow (infinite extent assumption for instance). Second, the sound treatment package in the cavity, usually an arrangement of various sound absorbing materials, is replaced by a single layer of fiberglass. Third, the presence of skin stringers is disregarded, because when stringer spacing and mount spacing are not integer multiples, the resulting periodic schemes would be too complex to take into account at this stage. Fourth, a diffuse field excitation is assumed although in real cruise flight conditions, the main excitation is the turbulent boundary layer (TBL). The vibratory response and radiation mechanisms of panels excited by a diffuse field and by a TBL are quite different [14] and a more realistic study should consider the TBL excitation case. Still, the presented diffuse field excitation study is useful since it represents a preliminary step to validate the model. Besides, this type of excitation is used in most transmission loss performance experiments and therefore remains of practical importance. Fifth, the influence of in plane tensions due to cabin pressurization is ignored for purposes of simplicity. These tensions are known for instance to raise the panel natural frequencies by adding rigidity to the system. Finally, the ring frames are considered transparent to the acoustic waves (cavity is not partitioned) because accounting for this feature requires the use of combined space harmonic/modal displacement fields [15]. Brunskog [15] showed that this assumption is valid when structure-borne transmission dominates over the airborne path. Yet, in his study, the cavity between the leaves was filled with air and not with fiberglass as in the present model. Knowing that the fiberglass will strongly damp the lateral reflections caused by the frames, it is thus reasonable to assume that the effects of the un-partitioned cavity hypothesis will remain small even in configurations where airborne transmission dominates.

The paper begins with a description of the geometry and the constants of the problem. Next, the equations of motion of the panels, the ring frames and the trim mounts are derived. Analytical expressions accelerating the solution of the whole system of equations are also given. For the numerical study, a description of the simulation parameters is first made. Then, the effects of mount stiffness, damping and spacing, of cavity absorption and of panel damping are presented and discussed. A section where the model is compared with finite elements simulations is also presented for validation. The paper ends by a summary of the major conclusions drawn from the parameters and validation studies and by giving perspectives for future work.

This study follows previous work of the authors on the effect of structural links in lightweight double panel structures [16]. The major recommendation in that article was that with lightweight partitions, the inertia and the resilience of the links significantly affect structure-borne transmission and therefore must be accounted for. This is the case in the proposed model. It should also be noted that studies similar to the present investigation were conducted by Craik and his collaborators [17–19], but in the context of building partitions and by using a SEA approach. The use of such an approach, i.e. an approach that does not account for the periodicity of the structure, was justified as follows in Ref. [18]: "Real structures are not sufficiently well built that they can be considered periodic and so many of the features predicted for periodic structures (with well defined dips and peaks) are also not observed. This approach is, therefore, of limited value for the study of real walls." If this is probably the case for building partitions, the tolerances are generally more severe in aerospace and the hypothesis of periodicity thus remains reasonable. Moreover, this hypothesis can be relaxed by averaging the transmissibility in third octave bands, which is the case in this paper.

2. The studied structure

2.1. Sub-systems description

A comprehensive diagram of the studied problem is shown in Fig. 1. The insulating structure is made of a skin (panel 1) ribbed by ring frames periodically spaced at a distance L_x. On each ring, the trim panel (panel 2) is attached by resilient

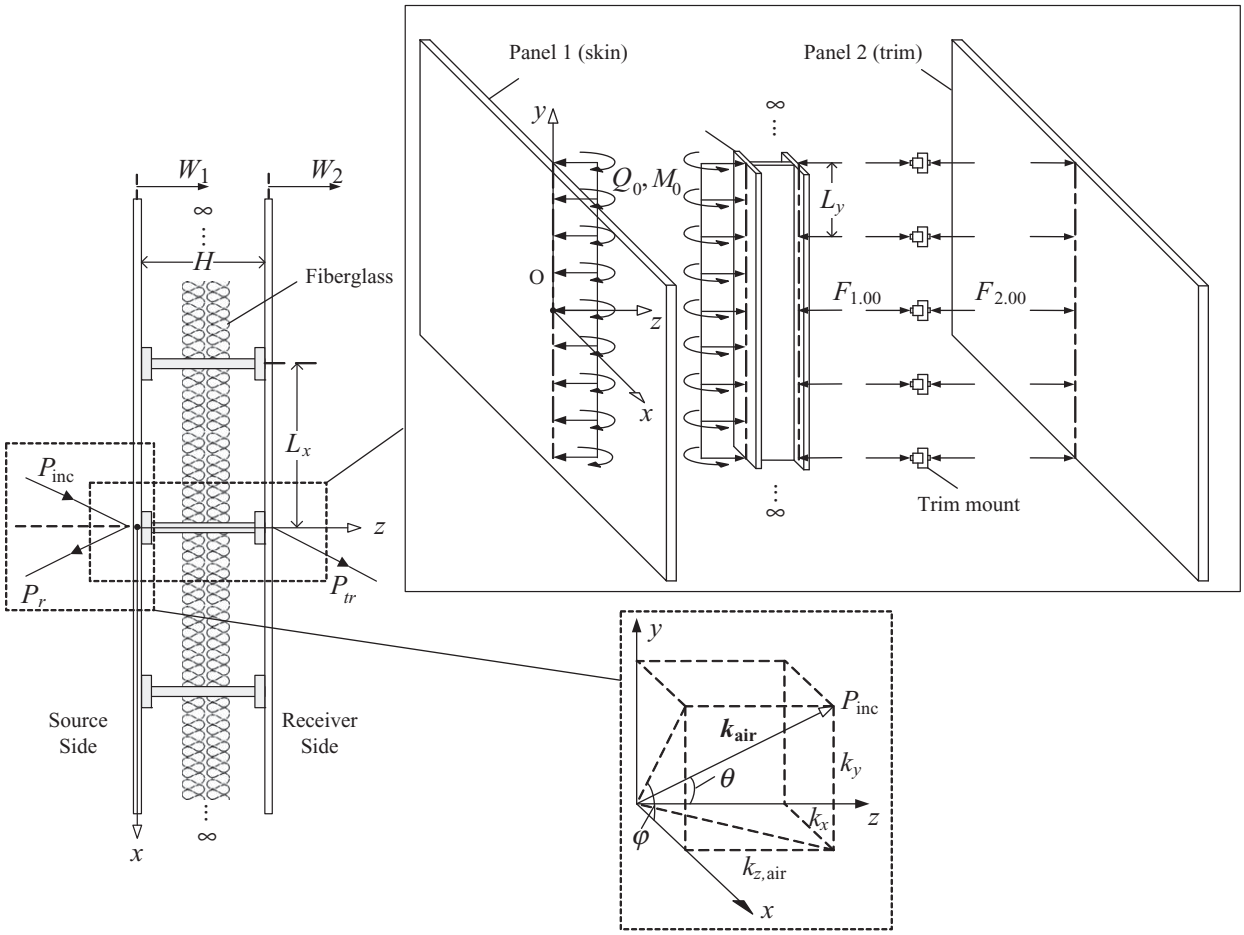

Fig. 1. Diagram of the problem.

mounts periodically spaced at a distance L_y. In Fig. 1, these frames have a symmetric I-shaped cross-section, which is the geometry studied in this paper. Usually, more sophisticated cross-section profiles are used to provide stiffness and resistance (e.g. Ω-shaped beams), but treating such geometries with precision would require more advanced models [20]. Finally, the cavity of width H between the panels is filled with a limp fibrous material. To account for the associated absorption, an equivalent fluid model [21] that makes use of the Biot's acoustical properties of the fiber is employed. Hence, the effective density of the fiberglass ρ_{cav} and the effective speed of sound and wavenumber c_{cav} and k_{cav} in the fiber ($k_{cav}=\omega/c_{cav}$) are complex and frequency dependent. On both sides of the partition, air with density ρ_{air} is present and the associated speed of sound and wavenumber are c_{air} and k_{air} ($=\omega/c_{air}$).

2.2. Acoustical excitation, fluid loading and reactions

On the source side, an acoustical plane wave P_{inc} impinges on the skin panel. The wave makes an angle θ (acoustic incident angle) with the z axis and its projection in the xy plane makes an angle φ (acoustic heading angle) with the x axis. Its amplitude is P_0 and its wavenumber $\boldsymbol{k}_{air}$ can be decomposed in the x, y and z directions:

$$P_{inc} = P_0 \exp(-jk_x x - jk_y y - jk_{z,air} z), \tag{1}$$

where

$$k_x = k_{air} \sin\theta \cos\varphi, \tag{2}$$

$$k_y = k_{air} \sin\theta \sin\varphi, \tag{3}$$

$$k_{z,air} = k_{air} \cos\theta. \tag{4}$$

The time dependence factor $\exp(j\omega t)$ was omitted in Eq. (1) and will henceforth be considered implicit. When it hits the partition, the incident wave creates a reflected wave P_r in the source region, a pressure P_{cav} inside the cavity and a transmitted wave P_{tr} on the receiver side. The displacements of the panels are noted W_1 and W_2. Since the rivets bonding the ring frames to the skin are closely spaced in aeronautic structures (typically less than 1 cm), a full line coupling is assumed between them. This approximation is valid at frequencies of interest, i.e. less than 10 kHz, because the effect of discrete fixing becomes significant only when half a bending wavelength of the plate fits between the rivets [18]. Therefore, between the skin and the pth ring frame located at $x=pL_x$, the force per unit length is Q_p and the moment per unit length in the y direction is M_p. On that same ring frame, the point force between the ring and the left side of the mount located at $y=qL_y$ is $F_{1,pq}$. Between the right side of the mount and the trim panel, the force is $F_{2,pq}$. The rotational coupling between the mounts, the ring frames and the trim panel is disregarded.

3. Derivation of the model

3.1. The panels and the cavity

The classical vibration analysis of metallic panels used in aeronautics usually requires only one degree of freedom due to their slight thickness ($\sim$1 mm), i.e. the transversal displacement W of the panel (thin plate in bending analysis). For a composite panel however, the necessary number of degrees of freedom depends upon its nature. For a composite panel with thin plies, the Kirchhoff–Love thin plate hypotheses can be applied (transverse shearing and rotational inertia are neglected) and three degrees of freedom are sufficient to describe its dynamics: the transverse displacement W and the membrane displacements of the panel's middle plane. This was the case in Yin et al.'s study [8] (Reddy's model [22] was used). On the other hand, when the panel has thick plies or a sandwich construction having a large shearing core (e.g. honeycomb cores), Reissner–Mindlin's first-order shear deformation assumptions are needed, and two additional degrees of freedom in rotation must be introduced, as in Berthelot's model [23]. In more advanced models [5–7], these five degrees of freedom are expanded for each layer of the laminate to account for thick skins.

In this paper, the formulation of the equations of motion of the panels are kept as general as possible so that both metallic and composite configurations can be handled. According to the problem statement made in Sections 2.1 and 2.2, the equations of motion of the skin and the trim are

$$\mathcal{D}_1[W_1(x,y)] = P_{inc}\|_{z=0} + P_r\|_{z=0} - P_{cav}\|_{z=0} - \sum_{p=-\infty}^{+\infty} Q_p(y)\delta(x-pL_x) + \frac{\partial}{\partial x}\left(\sum_{p=-\infty}^{+\infty} M_p(y)\delta(x-pL_x)\right), \tag{5}$$

$$\mathcal{D}_2[W_2(x,y)] = P_{cav}\|_{z=H} - P_{tr}\|_{z=H} + \sum_{p,q=-\infty}^{+\infty} F_{2,pq}\delta(x-pL_x)\delta(y-qL_y), \tag{6}$$

where $\mathcal{D}_1$ and $\mathcal{D}_2$ are the linear differential operators governing elastic and inertial forces in the skin and the trim panels, respectively. For an isotropic thin plate in bending, the operator D is given by

$$\mathcal{D} = D(1+j\eta)\left(\frac{\partial^4}{\partial x^4} + 2\frac{\partial^4}{\partial x^2\,\partial y^2} + \frac{\partial^4}{\partial y^4}\right) - m_s\omega^2, \tag{7}$$

where D, m_s and η, are respectively, the bending stiffness, the mass per unit area and the damping loss factor of the plate. For a composite panel, this formulation is not strictly rigorous since, as mentioned previously, more than one degree of freedom is necessary for its vibration analysis. However, as long as the transverse displacement of the whole panel is described by only one degree of freedom W in the model, i.e. that W is the same for each layer, the analysis is valid since the equivalent dynamic stiffness of the panel is obtainable for any arbitrary structural wave forcing propagation in the structure by using its dispersion relationships. Using Berthelot's model [23], Ghinet et al. [7] showed how to calculate the impedance associated with an acoustic wave impinging upon the composite panel. The same approach is used in this paper, but with an arbitrary structural wavenumber k_{str} and an arbitrary structural heading angle φ_{str}, i.e. a wavenumber and an angle that are not related to the incident acoustic wave. Therefore, by assuming space-harmonic expansion for the transverse displacements, the dynamic stiffness of the panel associated to each space-harmonic wave travelling in the structure can be derived (see Eq. (39)). The method is described in Appendix A. It is important to mention that employing Mace's [24] Fourier transform technique as Yin et al. [8] did would lead to equivalent results for the dynamic stiffness, but would also be more formal. Still, the present method is interesting since it allows the use of different models for the panels (for instance, in the parameters study, the skin is assumed composite while the trim is sandwich). It is also important to point out once more that the proposed approach cannot handle models involving more than one degree of freedom for the transversal displacement of the panel. With such models, the fluid loading pressures and the reactions of the ring frames and the mounts, depending on which side they are applied on the panels, would be associated either with the transverse displacement of the first layer, or with the transverse displacement of the last layer.

To alleviate the notation, let $\sum_{p=-\infty}^{p=+\infty} = \sum_p$ and $\sum_{q=-\infty}^{q=+\infty} = \sum_q$. Since the system is periodic in the xy plane, the displacements of the panels and the pressures are written in the form of two-dimensional space harmonic

series [25]:

$$W_1(x,y)=\sum_{pq}u_{1,pq}\exp(-\mathrm{j}\,k_{x,p}x-\mathrm{j}k_{y,q}y), \tag{8}$$

$$W_2(x,y)=\sum_{pq}u_{2,pq}\exp(-\mathrm{j}\,k_{x,p}x-\mathrm{j}k_{y,q}y), \tag{9}$$

$$P_r(x,y,z)=\sum_{pq}\varepsilon_{pq}\exp(-\mathrm{j}k_{x,p}x-\mathrm{j}k_{y,q}y+\mathrm{j}k_{z,\mathrm{air},pq}z), \tag{10}$$

$$P_{\mathrm{cav}}(x,y,z)=\sum_{pq}\alpha_{pq}\exp(-\mathrm{j}k_{x,p}x-\mathrm{j}k_{y,q}y-\mathrm{j}k_{z,\mathrm{cav},pq}z)+\beta_{pq}\exp(-\mathrm{j}k_{x,p}x-\mathrm{j}k_{y,q}y+\mathrm{j}k_{z,\mathrm{cav},pq}z), \tag{11}$$

$$P_{\mathrm{tr}}(x,y,z)=\sum_{pq}\xi_{pq}\exp(-\mathrm{j}k_{x,p}x-\mathrm{j}k_{y,q}y-\mathrm{j}k_{z,\mathrm{air},pq}z), \tag{12}$$

where

$$k_{x,p}=k_x+2p\pi/L_x, \tag{13}$$

$$k_{y,q}=k_y+2q\pi/L_y, \tag{14}$$

$$k_{z,\mathrm{air},pq}=\sqrt{k_{\mathrm{air}}^2-k_{x,p}^2-k_{y,q}^2}, \tag{15}$$

$$k_{z,\mathrm{cav},pq}=\sqrt{k_{\mathrm{cav}}^2-k_{x,p}^2-k_{y,q}^2}. \tag{16}$$

The series are truncated to a finite but sufficient number of terms p and q to ensure convergence at the highest frequency of interest (10 kHz in this paper), i.e. $p=[-p_{\max},\,-p_{\max}+1,\ldots,\,p_{\max}-1,\,p_{\max}]$ and $q=[-q_{\max},\,-q_{\max}+1,\ldots,\,q_{\max}-1,\,q_{\max}]$. Given the periodic nature of the structure, $F_{1,pq}$, $F_{2,pq}$, $Q_p(y)$ and $M_p(y)$ can be expressed in terms of $F_{1,00}$, $F_{2,00}$, $Q_0(y)$ and $M_0(y)$, respectively [24]:

$$F_{i,pq}=F_{i,00}\exp(-\mathrm{j}k_xpL_x)\exp(-\mathrm{j}k_yqL_y),\quad i=1,2, \tag{17}$$

$$Q_p(y)=Q_0(y)\exp(-\mathrm{j}k_xpL_x), \tag{18}$$

$$M_p(y)=M_0(y)\exp(-\mathrm{j}k_xpL_x). \tag{19}$$

Moreover, the assumed displacements imply that the force and the moment per unit length $Q_p(y)$ and $M_p(y)$ applied by the pth ring frame on the skin can also be expanded as a sum of space harmonics:

$$Q_p(y)=\sum_q Q_{pq}\exp(-\mathrm{j}k_{y,q}y), \tag{20}$$

$$M_p(y)=\sum_q M_{pq}\exp(-\mathrm{j}k_{y,q}y). \tag{21}$$

Since Poisson's formula allows writing the sum of the δ functions as follows:

$$\sum_p\delta(x-pL_x)=\frac{1}{L_x}\sum_p\exp\left(\frac{-2\mathrm{j}p\pi x}{L_x}\right), \tag{22}$$

$$\sum_q\delta(y-qL_y)=\frac{1}{L_y}\sum_q\exp\left(\frac{-2\mathrm{j}q\pi y}{L_y}\right), \tag{23}$$

combining Eqs. (17)–(23) yields:

$$\sum_{pq}F_{i,pq}\delta(x-pL_x)\delta(y-qL_y)=\frac{F_{i,00}}{L_xL_y}\sum_{pq}\exp(-\mathrm{j}k_{x,p}x)\exp(-\mathrm{j}k_{y,q}y),\quad i=1,2, \tag{24}$$

$$\sum_p Q_p(y)\delta(x-pL_x)=\frac{1}{L_x}\sum_{pq}Q_{0q}\exp(-\mathrm{j}k_{y,q}y)\exp(-\mathrm{j}k_{x,p}x), \tag{25}$$

$$\sum_p M_p(y)\delta(x-pL_x)=\frac{1}{L_x}\sum_{pq}M_{0q}\exp(-\mathrm{j}k_{y,q}y)\exp(-\mathrm{j}k_{x,p}x). \tag{26}$$

As well, continuity at fluid–panel interfaces requires that

$$\left.\frac{\partial(P_{\text{inc}}+P_{\text{r}})}{\partial z}\right|_{z=0} = \omega^2 \rho_{\text{air}} W_1, \tag{27}$$

$$\left.\frac{\partial P_{\text{cav}}}{\partial z}\right|_{z=0} = \omega^2 \rho_{\text{cav}} W_1, \tag{28}$$

$$\left.\frac{\partial P_{\text{cav}}}{\partial z}\right|_{z=H} = \omega^2 \rho_{\text{cav}} W_2, \tag{29}$$

$$\left.\frac{\partial P_{\text{tr}}}{\partial z}\right|_{z=H} = \omega^2 \rho_{\text{air}} W_2. \tag{30}$$

Substituting Eqs. (8)–(12) into Eqs. (27)–(30) and utilizing the fact that the continuity equations (in the form of sums) must be true for all values of x and y, the pressure coefficients and displacement amplitude coefficients are related for each combination pq by

$$\varepsilon_{pq} = P_0 \delta_{pq} - \frac{\mathrm{j}\omega^2 \rho_{\text{air}} u_{1,pq}}{k_{z,\text{air},pq}}, \tag{31}$$

$$\alpha_{pq} = \frac{\omega^2 \rho_{\text{cav}} \csc(k_{z,\text{cav},pq} H)}{2k_{z,\text{cav},pq}} (\exp(\mathrm{j}k_{z,\text{cav},pq} H) u_{1,pq} - u_{2,pq}), \tag{32}$$

$$\beta_{pq} = \frac{\omega^2 \rho_{\text{cav}} \csc(k_{z,\text{cav},pq} H)}{2k_{z,\text{cav},pq}} (\exp(-\mathrm{j}k_{z,\text{cav},pq} H) u_{1,pq} - u_{2,pq}), \tag{33}$$

$$\xi_{pq} = \frac{\mathrm{j}\omega^2 \rho_{\text{air}} \exp(\mathrm{j}k_{z,\text{air},pq} H) u_{2,pq}}{k_{z,\text{air},pq}}, \tag{34}$$

where $\delta_{00}=1$ and $\delta_{pq}=0$ for $p\neq 0$ or $q\neq 0$. Inserting Eqs. (24)–(26) and (31)–(34) into Eqs. (5) and (6) and requiring the sums to be true for all values of x and y, two coupled linear equations are obtained for each combination pq:

$$\begin{bmatrix} K_{11,pq} & K_{12,pq} \\ K_{21,pq} & K_{22,pq} \end{bmatrix} \begin{bmatrix} u_{1,pq} \\ u_{2,pq} \end{bmatrix} = \begin{bmatrix} 2P_0\delta_{pq} - Q_{0q}/L_x - \mathrm{j}k_{x,p} M_{0q}/L_x \\ F_{2,00}/L_x L_y \end{bmatrix}, \tag{35}$$

where

$$K_{11,pq} = K_{\text{panel},1,pq} + \frac{\mathrm{j}\omega^2 \rho_{\text{air}}}{k_{z,\text{air},pq}} + \frac{\omega^2 \rho_{\text{cav}} \cot(k_{z,\text{cav},pq} H)}{k_{z,\text{cav},pq}}, \tag{36}$$

$$K_{22,pq} = K_{\text{panel},2,pq} + \frac{\mathrm{j}\omega^2 \rho_{\text{air}}}{k_{z,\text{air},pq}} + \frac{\omega^2 \rho_{\text{cav}} \cot(k_{z,\text{cav},pq} H)}{k_{z,\text{cav},pq}}, \tag{37}$$

$$K_{12,pq} = K_{21,pq} = -\frac{\omega^2 \rho_{\text{cav}} \csc(k_{z,\text{cav},pq} H)}{k_{z,\text{cav},pq}}. \tag{38}$$

In Eqs. (36) and (37), $K_{\text{panel},1,pq}$ and $K_{\text{panel},2,pq}$ represent the dynamic stiffness of the equivalent panels associated to the pqth space harmonic. For a composite panel, this stiffness is function of the angular frequency ω and of the structural wavenumber $k_{\text{str},pq}$ and structural heading angle $\varphi_{\text{str},pq}$ associated with the pqth space harmonic:

$$K_{\text{panel},i,pq} = f(\omega, k_{\text{str},pq}, \varphi_{\text{str},pq}), \quad i = 1, 2, \tag{39}$$

where

$$k_{\text{str},pq}^2 = k_{x,p}^2 + k_{y,q}^2, \tag{40}$$

$$\varphi_{\text{str},pq} = \arctan(k_{y,q}/k_{x,p}). \tag{41}$$

$K_{\text{panel},i,pq}$ can be derived by using the dispersion relationships of the panels as shown in Appendix A. An interesting strategy to reduce computation time is to build a matrix containing the dynamic stiffness of the panel prior to the main calculations (the matrix is three-dimensional since K_{panel} is function of ω, $k_{\text{str},pq}$ and $\varphi_{\text{str},pq}$). Once it has been built for structural heading angles ranging between 0 and 2π, for all frequencies of interest and for sufficiently high structural wavenumbers knowing that p varies from $-p_{\max}$ to $p_{\max}$ and q from $-q_{\max}$ to $q_{\max}$, the dynamic stiffness of the panel associated with the pqth space harmonic is easily obtained by interpolating within that matrix. For an

isotropic thin plate in bending, the dynamic stiffness is independent of the structural heading angle and is given by

$$K_{\text{panel},pq} = D(1+\mathrm{j}\eta)k_{\text{str},pq}^4 - m_s\omega^2. \tag{42}$$

By manipulating Eq. (35), explicit expressions of $u_{1,pq}$ and $u_{2,pq}$ are obtained:

$$u_{1,pq} = 2P_0 C_{11,pq}\delta_{pq} - \frac{C_{11,pq}}{L_x}Q_{0q} - \frac{\mathrm{j}k_{x,p}C_{11,pq}}{L_x}M_{0q} + \frac{C_{12,pq}}{L_xL_y}F_{2,00}, \tag{43}$$

$$u_{2,pq} = 2P_0 C_{21,pq}\delta_{pq} - \frac{C_{21,pq}}{L_x}Q_{0q} - \frac{\mathrm{j}k_{x,p}C_{21,pq}}{L_x}M_{0q} + \frac{C_{22,pq}}{L_xL_y}F_{2,00}, \tag{44}$$

where

$$\begin{bmatrix} C_{11,pq} & C_{12,pq} \\ C_{21,pq} & C_{22,pq} \end{bmatrix} = \begin{bmatrix} K_{11,pq} & K_{12,pq} \\ K_{21,pq} & K_{22,pq} \end{bmatrix}^{-1}. \tag{45}$$

3.2. The ring frames and the trim mounts

For the ring frames, simple Euler–Bernoulli beam modeling is considered. Moreover, translation and torsion motions are assumed to be decoupled (eccentricity is disregarded). Therefore, the equations of motion in translation and rotation for the ring frame located at x=0 are, respectively [26]

$$\sum_q Q_{0q}\exp(-\mathrm{j}k_{y,q}y) - \sum_q F_{1,0q}\delta(y-qL_y) = \left(\{EI_x\}_{\text{eq}}\frac{\partial^4}{\partial y^4} - m_B'\,\omega^2\right)W_{B,0}, \tag{46}$$

$$\sum_q M_{0q}\exp(-\mathrm{j}k_{y,q}y) = \left(\{EI_\omega\}_{\text{eq}}\frac{\partial^4}{\partial y^4} - \{GJ_y\}_{\text{eq}}\frac{\partial^2}{\partial y^2} - I_O\omega^2\right)\phi_{B,0}, \tag{47}$$

where $\{EI_x\}_{\text{eq}}$ is the equivalent bending stiffness of the beam with respect to the x axial axis, $\{EI_\omega\}_{\text{eq}}$ its equivalent warping stiffness, $\{GJ_y\}_{\text{eq}}$ its equivalent torsional stiffness with respect to the y axial axis, m_B' its mass per unit length and I_O its moment of inertia per unit length with respect to the centroidal axial axis. Continuity between the displacements of the ring frames and the skin (line coupling condition) allows writing the translational displacement $W_{B,0}$ and the torsion angle $\phi_{B,0}$ of the ring frame located at x=0 as a function of the skin's displacement:

$$W_{B,0} = W_1\|_{x=0} = \sum_{pq} u_{1,pq}\exp(-\mathrm{j}k_{y,q}y), \tag{48}$$

$$\phi_{B,0} = \left.\frac{\partial W_1}{\partial x}\right\|_{x=0} = \sum_{pq} -\mathrm{j}k_{x,p}u_{1,pq}\exp(-\mathrm{j}k_{y,q}y). \tag{49}$$

Knowing that Eqs. (46) and (47) must be true for all values of y, the following relationships are obtained for each q by considering Eqs. (24)–(26) and (46)–(49):

$$Q_{0q} - \frac{F_{1,00}}{L_y} = K_{BT,q}\sum_p u_{1,pq}, \tag{50}$$

$$M_{0q} = K_{BR,q}\sum_p -\mathrm{j}k_{x,p}u_{1,pq}, \tag{51}$$

where

$$K_{BT,q} = \{EI_x\}_{\text{eq}}k_{y,q}^4 - m_B'\,\omega^2, \tag{52}$$

$$K_{BR,q} = \{EI_\omega\}_{\text{eq}}k_{y,q}^4 + \{GJ_y\}_{\text{eq}}k_{y,q}^2 - I_O\omega^2. \tag{53}$$

For the trim mounts, the force and the displacement on the left side of each mount can be linked to the force and the displacement on its right side by a dynamic transfer matrix **T** (four pole formulation). For the mount located at x=0 and y=0, this yields

$$\begin{bmatrix} F_{1,00} \\ W_{B,0}\|_{y=0} \end{bmatrix} = \begin{bmatrix} F_{1,00} \\ W_1\|_{x,y=0} \end{bmatrix} = \begin{bmatrix} T_{11} & T_{12} \\ T_{21} & T_{22} \end{bmatrix}\begin{bmatrix} F_{2,00} \\ W_2\|_{x,y=0} \end{bmatrix}. \tag{54}$$

The terms in the matrix **T** are usually derived experimentally for elastomeric mounts [27], but in this study, the mounts are modeled by a lumped mass-spring-mass system. The total mass of the mount m_{mount} is split equally between the two lumped masses ($m_{\text{mount}}/2$) and the spring's stiffness of the mount is K_{mount}. Structural damping is introduced through the

loss factor η_{mount}. The **T** matrix thus takes the following form:

$$\mathbf{T}=\begin{bmatrix} T_{11} & T_{12} \\ T_{21} & T_{22} \end{bmatrix}=\begin{bmatrix} 1-\dfrac{m_{\text{mount}}\omega^2}{2K^*_{\text{mount}}} & -m_{\text{mount}}\omega^2\left(1-\dfrac{m_{\text{mount}}\omega^2}{4K^*_{\text{mount}}}\right) \\ \dfrac{1}{K^*_{\text{mount}}} & 1-\dfrac{m_{\text{mount}}\omega^2}{2K^*_{\text{mount}}} \end{bmatrix}, \tag{55}$$

$$K^*_{\text{mount}}=K_{\text{mount}}(1+\mathrm{j}\eta_{\text{mount}}). \tag{56}$$

The following relationship is obtained through manipulation of Eq. (54):

$$\begin{bmatrix} W_1\|_{x,y=0} \\ W_2\|_{x,y=0} \end{bmatrix}=\begin{bmatrix} \sum_{pq} u_{1,pq} \\ \sum_{pq} u_{2,pq} \end{bmatrix}=\begin{bmatrix} T_{22}/T_{12} & T_{21}-T_{11}T_{22}/T_{12} \\ 1/T_{12} & -T_{11}/T_{12} \end{bmatrix}\begin{bmatrix} F_{1,00} \\ F_{2,00} \end{bmatrix}=\begin{bmatrix} A_{11} & A_{12} \\ A_{21} & A_{22} \end{bmatrix}\begin{bmatrix} F_{1,00} \\ F_{2,00} \end{bmatrix}=\mathbf{A}\begin{bmatrix} F_{1,00} \\ F_{2,00} \end{bmatrix}. \tag{57}$$

3.3. Expression for the transmission loss

The number of linearly independent equations now matches the number of unknowns. However, to decrease computation time, the size of the system must be reduced. First, by summing Eq. (43) over all values of p and combining the result with Eqs. (50) and (51), Q_{0q} and M_{0q} can be expressed in function of $F_{1,00}$ and $F_{2,00}$:

$$\begin{bmatrix} Q_{0q} \\ M_{0q} \end{bmatrix}=2P_0\delta_q\begin{bmatrix} \kappa_{1,q} \\ \kappa_{2,q} \end{bmatrix}+\begin{bmatrix} \psi_{11,q} & \psi_{12,q} \\ \psi_{21,q} & \psi_{22,q} \end{bmatrix}\begin{bmatrix} F_{1,00} \\ F_{2,00} \end{bmatrix}, \tag{58}$$

where

$$\begin{bmatrix} \kappa_{1,q} \\ \kappa_{2,q} \end{bmatrix}=\begin{bmatrix} \chi_{11,q} & \chi_{12,q} \\ \chi_{21,q} & \chi_{22,q} \end{bmatrix}\begin{bmatrix} C_{11,0q} \\ -\mathrm{j}k_{x,0}C_{11,0q} \end{bmatrix}, \tag{59}$$

$$\begin{bmatrix} \psi_{11,q} & \psi_{12,q} \\ \psi_{21,q} & \psi_{22,q} \end{bmatrix}=\begin{bmatrix} \chi_{11,q} & \chi_{12,q} \\ \chi_{21,q} & \chi_{22,q} \end{bmatrix}\begin{bmatrix} \dfrac{1}{K_{BT,q}L_y} & \sum\limits_p \dfrac{C_{12,pq}}{L_xL_y} \\ 0 & -\sum\limits_p \dfrac{\mathrm{j}k_{x,p}C_{12,pq}}{L_xL_y} \end{bmatrix}, \tag{60}$$

$$\begin{bmatrix} \chi_{11,q} & \chi_{12,q} \\ \chi_{21,q} & \chi_{22,q} \end{bmatrix}=\begin{bmatrix} \dfrac{1}{K_{BT,q}}+\sum\limits_p \dfrac{C_{11,pq}}{L_x} & \sum\limits_p \dfrac{\mathrm{j}k_{x,p}C_{11,pq}}{L_x} \\ -\sum\limits_p \dfrac{\mathrm{j}k_{x,p}C_{11,pq}}{L_x} & \dfrac{1}{K_{BR,q}}+\sum\limits_p \dfrac{k^2_{x,p}C_{11,pq}}{L_x} \end{bmatrix}^{-1}, \tag{61}$$

with δ_0=1 and δ_q=0 for $q\neq 0$. Summing Eqs. (43) and (44) over all ps and qs by replacing Q_{0q} and M_{0q} with Eq. (58) yields

$$\begin{bmatrix} \sum_{pq} u_{1,pq} \\ \sum_{pq} u_{2,pq} \end{bmatrix}=\begin{bmatrix} S_{11} & S_{12} \\ S_{21} & S_{22} \end{bmatrix}\begin{bmatrix} F_{1,00} \\ F_{2,00} \end{bmatrix}+\begin{bmatrix} G_1 \\ G_2 \end{bmatrix}=\mathbf{SF}+\mathbf{G}, \tag{62}$$

where

$$S_{i1}=-\frac{1}{L_x}\sum_q\left(\psi_{11,q}\sum_p C_{i1,pq}+\psi_{21,q}\sum_p \mathrm{j}k_{x,p}C_{i1,pq}\right), \quad i=1,2, \tag{63}$$

$$S_{i2}=-\frac{1}{L_x}\sum_q\left(\psi_{12,q}\sum_p C_{i1,pq}+\psi_{22,q}\sum_p \mathrm{j}k_{x,p}C_{i1,pq}\right)+\frac{1}{L_xL_y}\sum_{pq} C_{i2,pq}, \quad i=1,2, \tag{64}$$

$$G_i=2P_0\left(C_{i1,00}-\kappa_{1,0}\sum_p \frac{C_{i1,p0}}{L_x}-\kappa_{2,0}\sum_p \frac{\mathrm{j}k_{x,p}C_{i1,p0}}{L_x}\right), \quad i=1,2. \tag{65}$$

Combining Eqs. (57) and (62), a system of equations is obtained and solved for $F_{1,00}$ and $F_{2,00}$:

$$[\mathbf{A}-\mathbf{S}]\mathbf{F}=\mathbf{G}. \tag{66}$$

With $F_{1,00}$ and $F_{2,00}$, Q_{0q} and M_{0q} can be calculated for each q from Eq. (58). The reactions Q_{0q}, M_{0q}, and $F_{2,00}$ are then substituted back into Eqs. (43) and (44) to find $u_{1,pq}$ and $u_{2,pq}$ for each p and q. The coefficients ξ_{pq} of the transmitted

pressure are then obtained through Eq. (34) and used to calculate the oblique transmission coefficient $\tau(\theta,\varphi)$ of the periodic model:

$$\tau(\theta,\varphi)=\frac{\sum_{pq}|\xi_{pq}|^2\,\mathrm{Re}\{k_{z,\mathrm{air},pq}\}}{|P_0|^2 k_{z,\mathrm{air}}}. \tag{67}$$

The diffuse field transmission coefficient τ_d is finally calculated by integrating $\tau(\theta,\varphi)$ over the acoustic incident angle θ and acoustic heading angle φ [28]:

$$\tau_d=\frac{\int_0^{2\pi}\int_0^{\theta_{\mathrm{lim}}}\tau(\theta,\varphi)\sin\theta\cos\theta\,\mathrm{d}\theta\,\mathrm{d}\varphi}{\int_0^{2\pi}\int_0^{\theta_{\mathrm{lim}}}\sin\theta\cos\theta\,\mathrm{d}\theta\,\mathrm{d}\varphi}=\frac{1}{\pi}\frac{\int_0^{\pi}\int_0^{\theta_{\mathrm{lim}}}\tau(\theta,\varphi)\sin\theta\cos\theta\,\mathrm{d}\theta\,\mathrm{d}\varphi}{\int_0^{\theta_{\mathrm{lim}}}\sin\theta\cos\theta\,\mathrm{d}\theta}, \tag{68}$$

and is used in the transmission loss (TL) formula:

$$\mathrm{TL}=-10\log_{10}(\tau_d). \tag{69}$$

Note that field incidence is considered in this paper, i.e. $\theta_{\mathrm{lim}}=78^\circ$ [28].

4. Numerical results

4.1. Simulation parameters

This section lists the parameters that are used throughout the numerical study. Two configurations are investigated: a configuration where the skin panel is metallic and another where it is composite. A composite sandwich is used for the trim panel in both configurations. Table 1 presents the properties of the materials used for the panels. In the metallic configuration, the skin is a 1 mm isotropic thin plate made of material 1 (aluminum). The ring frames, also made of material 1, have a web length of 47 mm, a flange length of 38 mm and a wall thickness of 3 mm. Calculation of the beam properties associated with these frames is made using textbook formulas [29].

For the composite configuration simulation, the skin is a symmetric laminate made from seven 0.25 mm layers of material 2, which gives a surface mass almost equal to the metallic case. The ply angle sequence is $0^\circ/45^\circ/-45^\circ/90^\circ/-45^\circ/45^\circ/0^\circ$ (the ply angle is defined in the same way as the acoustic heading angle φ). This time, the frames are made from three composite sub-panels (two horizontal for the flanges and one vertical for the web) that are exactly equivalent to the skin panel except that every layer thickness is doubled to 0.5 mm to provide stiffness (the wall thickness of the frames is therefore 3.5 mm). The web and flange lengths of the frames are kept at 47 and 38 mm. Lee and Kim [30] showed how to calculate the equivalent beam properties of these constructions. Finally, the trim is a symmetric sandwich panel with a 12.7 mm thick core of material 3 and with 1.2 mm thick skins made of material 4. The three layers have a 0° ply angle orientation. It should be noted that the model presented by Ghinet and Atalla [6,31] is used in the derivation of the dynamic stiffness matrix of the trim instead of using Berthelot's model [23] as for the skin (the procedure detailed in Appendix A remains the same even if the dispersion equations are different). This model assumes the trim's skins to be composite and accounts for orthotropic cores. It has been shown both experimentally and numerically to apply well for sandwich structures where dilatational motion is not perceptible at the audible frequencies of interest [31,32].

For the fiberglass filling the cavity, the Biot's acoustical properties given in Table 2 are used. These are values representative of typical aircraft fiberglass grades. The numerical constants for air on both sides of the partition are $\rho_{\mathrm{air}}=1.21\,\mathrm{kg\,m^{-3}}$ and $c_{\mathrm{air}}=342\,\mathrm{m\,s^{-1}}$; the width H of the cavity is 50.8 mm (2 in) and the ring frame and trim mount spacing L_x and L_y are 762 mm (30 in) and 305 mm (12 in). For the mounts, a mass of 0.01 kg is considered. The mount structural damping varies between 1 percent and 50 percent and the stiffness between 10^4 and $10^7\,\mathrm{N\,m^{-1}}$.

Simulations are done in one twelfth octave bands for frequencies ranging from 100 Hz to 10 kHz and the diffuse field transmissibility is averaged in third octave bands to smooth the TL fluctuations caused by the pass and stop bands characteristic of periodic structures [33]. Finally, $p_{\max}$ and $q_{\max}$ are set to 45 and 20 to reach a satisfactory level of convergence, i.e. less than 1 percent of difference in the TL curve up to 10 kHz if $p_{\max}$ and $q_{\max}$ are both raised by five (i.e. 50 and 25, respectively).

Table 1
Material properties used for the panels.

Property	Material 1	Material 2	Material 3	Material 4
Young modulus—x direction (Pa)	70×10^9	1.25×10^{11}	0.1448×10^9	0.48×10^{11}
Young modulus—y direction (Pa)	70×10^9	10×10^9	0.1448×10^9	0.48×10^{11}
Shear modulus—xy plane (Pa)	26.3×10^9	5.9×10^9	0.5×10^8	0.181×10^{11}
Shear modulus—xz plane (Pa)	26.3×10^9	3×10^9	0.5×10^8	0.2757×10^{10}
Shear modulus—yz plane (Pa)	26.3×10^9	5.9×10^9	0.5×10^8	0.2757×10^{10}
Poisson's ratio—xy plane	0.33	0.4	0.45	0.30
Density ($\mathrm{kg\,m^{-3}}$)	2750	1600	110.44	1550
Damping loss factor	1%	1%	1%	1%

Table 2
Dynamic properties of the fibrous material (property, value).

Density of the fluid phase	$1.21\,kg\,m^{-3}$	Tortuosity	1.25
Speed of sound in the fluid phase	$342\,m\,s^{-1}$	Viscous length	$50\times10^{-6}\,m$
Flow resistivity	$20\,000\,Ns\,m^{-4}$	Thermal length	$100\times10^{-6}\,m$
Porosity	0.94	Density of the solid phase	$5.5\,kg\,m^{-3}$

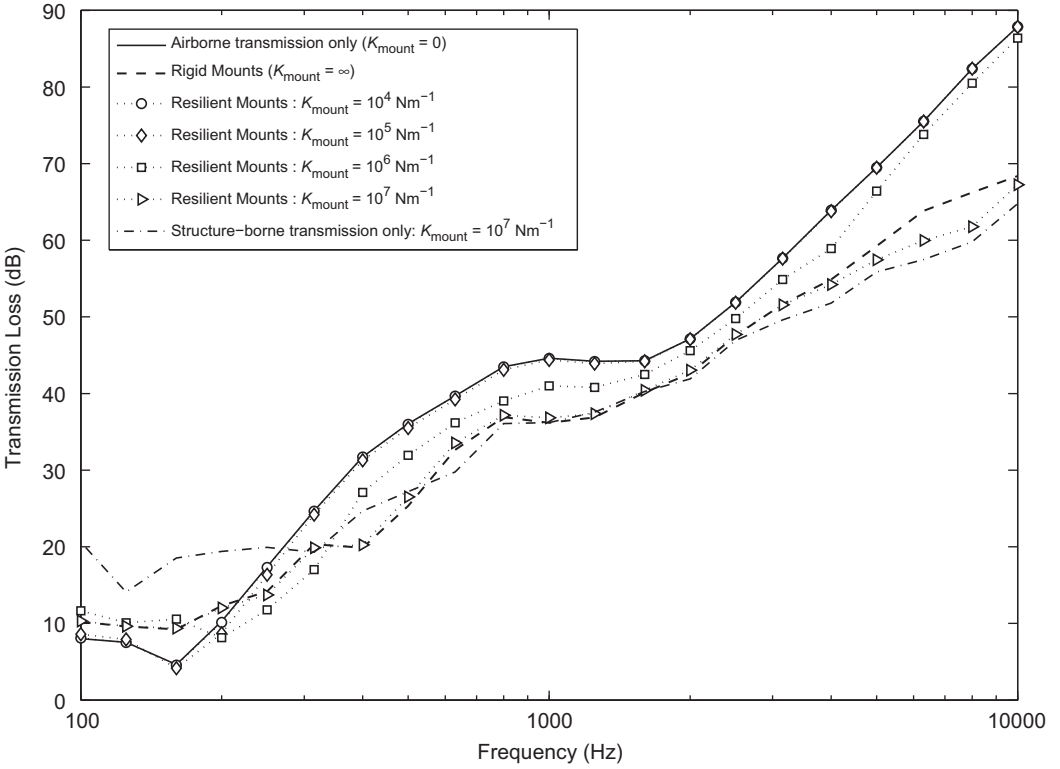

Fig. 2. The influence of mount stiffness (metallic configuration).

4.2. The influence of mount stiffness

Figs. 2 and 3 present the calculated results for the metallic and composite configurations, respectively. Seven curves are plotted in each figure: a curve showing the airborne transmission only (the mounts are perfectly resilient in that case, i.e. $K_{mount}=0$), a curve where the mounts are perfectly rigid ($K_{mount}=\infty$), four other curves where mount stiffness varies between 10^4 and $10^7\,Nm^{-1}$ and where the structural loss factor is 1 percent and finally, a curve showing structure-borne transmission only for $K_{mount}=10^7\,Nm^{-1}$. This last curve was obtained by inhibiting the fluid coupling between the panels (vacuum inside the cavity) and is presented to show the regions of dominance of structure-borne vs. airborne transmission.

Below 4 kHz, the results for the metallic and the composite configurations are almost identical, as their skins have similar surface masses. Moreover, the dip associated with the critical frequency of the trim panel is observed at 1.6 kHz for the two curves. However, above 4 kHz, the critical frequency of the composite skin panel occurring at 8 kHz creates appreciable differences between the two cases (up to 15 dB at 10 kHz). The dips seen at 400 Hz in both cases, at 6.3 kHz for the composite case and at 8 kHz for the metallic case are caused by the periodic nature of the structure, i.e. that pass bands of important magnitude are present in the third-octave band associated with these frequencies. This reduces the global energy of the band when the transmissibility is averaged.

At low frequencies ($f<300$ Hz), the additional stiffness provided by the perfectly rigid mounts and by mounts with $K_{mount}=10^6$ and $10^7\,Nm^{-1}$ increases the TL by concealing the mass-air-mass resonance [28] of the double-wall partition. This resonance occurs at 160 Hz for perfectly resilient mounts and for $K_{mount}=10^4$ and $10^5\,Nm^{-1}$. On the contrary, the mount stiffness has a deleterious effect on the TL at mid and high frequencies: as the latter increases, the TL decreases. This is because the structure-borne path starts to dominate over the airborne path (up to 20 dB of difference between the perfectly rigid and perfectly resilient mounts). It is also observed that when structure-borne transmission dominates with

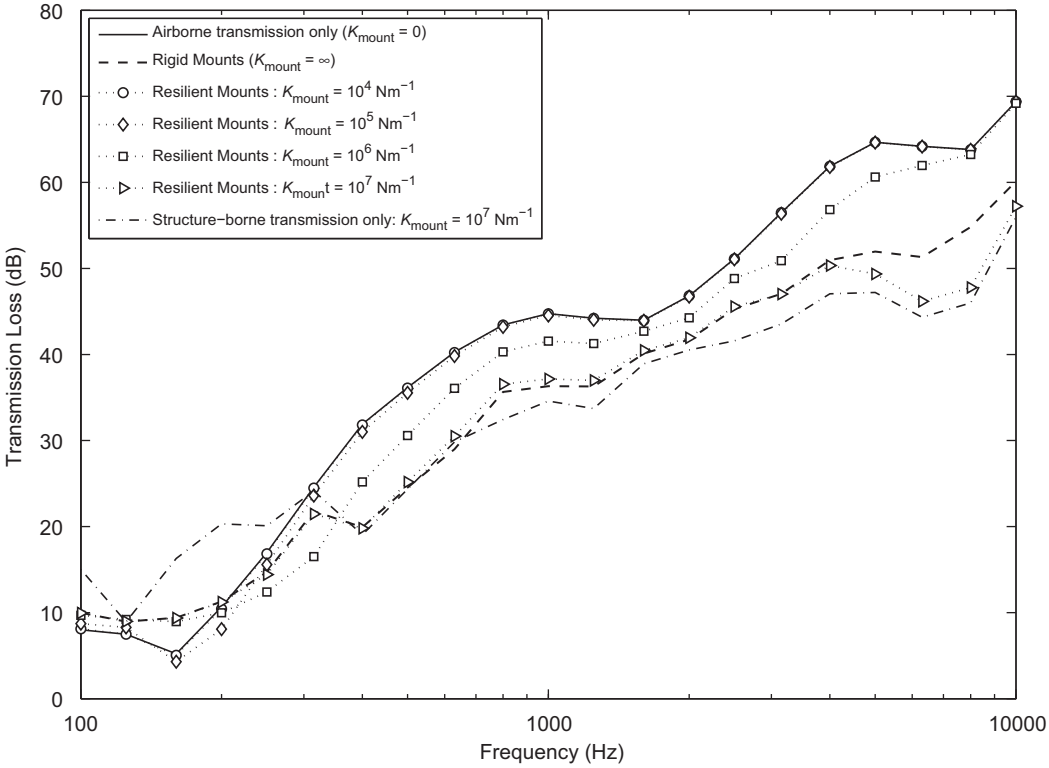

Fig. 3. The influence of mount stiffness (composite configuration).

$K_{\text{mount}}=10^7\,\text{Nm}^{-1}$, the additional equivalent mass and damping provided by the fiberglass inside the cavity results in a higher TL for the total transmission than the TL for structure-borne transmission alone. With $K_{\text{mount}}=10^5\,\text{Nm}^{-1}$, almost complete structural insulation is reached for frequencies of interest. Therefore, lowering the stiffness to $10^4\,\text{Nm}^{-1}$ has practically no effect since airborne transmission already dominates. To exploit its full potential, a mount with a stiffness of $10^4\,\text{Nm}^{-1}$ would have to be used with a fiber with greater absorption.

With $K_{\text{mount}}=10^6\,\text{Nm}^{-1}$, the TL is higher than with rigid mounts over the entire spectrum except for frequencies ranging between 200 and 315 Hz. The same behavior is observed with $K_{\text{mount}}=10^7\,\text{Nm}^{-1}$ (the TL is slightly higher on the whole frequency range except between 4 and 10 kHz). To explain these counterintuitive results, i.e. to explain why the TL with resilient mounts can go under the TL with rigid mounts, an analysis based on Fahy's assumptions for structure-borne sound in mechanically coupled double leaf partitions can be exploited [28]. First, let $v_{\text{mount},1}$ and $v_{\text{mount},2}$ be the velocities of the first and the second panel at the mount location and $Z_{p,1}$ and $Z_{p,2}$ be the local driving point impedances. Then, assume that the motion of each mount is independent of any other. Finally, let v_1 be the global velocity of the first panel far from the mounts. The driving force exerted on a mount by the first panel is therefore given by $Z_{p,1}(v_1-v_{\text{mount},1})$ and the equations of motion for the two lumped masses of the mount, are respectively,

$$\text{j}\omega\frac{m_{\text{mount}}}{2}v_{\text{mount},1}=\frac{K^*_{\text{mount}}}{\text{j}\omega}(v_{\text{mount},2}-v_{\text{mount},1})+Z_{p,1}(v_1-v_{\text{mount},1}), \tag{70}$$

$$\text{j}\omega\frac{m_{\text{mount}}}{2}v_{\text{mount},2}=\frac{K^*_{\text{mount}}}{\text{j}\omega}(v_{\text{mount},1}-v_{\text{mount},2})-Z_{p,2}v_{\text{mount},2}. \tag{71}$$

Combining Eqs. (70) and (71) yields the following velocity ratio $v_{\text{mount},2}/v_1$:

$$\frac{v_{\text{mount},2}}{v_1}=\frac{Z_{p,1}}{(Z_{p,1}+Z_{p,2})\left(1-\frac{m_{\text{mount}}\omega^2}{2K^*_{\text{mount}}}\right)+\frac{\text{j}\omega Z_{p,1}Z_{p,2}}{K^*_{\text{mount}}}+\text{j}\omega m_{\text{mount}}\left(1-\frac{m_{\text{mount}}\omega^2}{4K^*_{\text{mount}}}\right)}. \tag{72}$$

Even if it is based on simplified reasoning, this ratio gives a good retrospective view of the parameters influencing structure-borne transmission. It shows that structural transmissibility with flexible mounts can be higher than with rigid mounts since the amplitude of the ratio at Eq. (72) is not necessarily maximal for $K_{\text{mount}}=\infty$. Moreover, it shows that this maximum value will not exactly occur at the resonance frequency of the mass-spring-mass system due to the interaction of the mounts with the panels (for $K_{\text{mount}}=10^6\,\text{Nm}^{-1}$ and $m_{\text{mount}}=0.01$ kg, the mass-spring-mass frequency is 3.2 kHz).

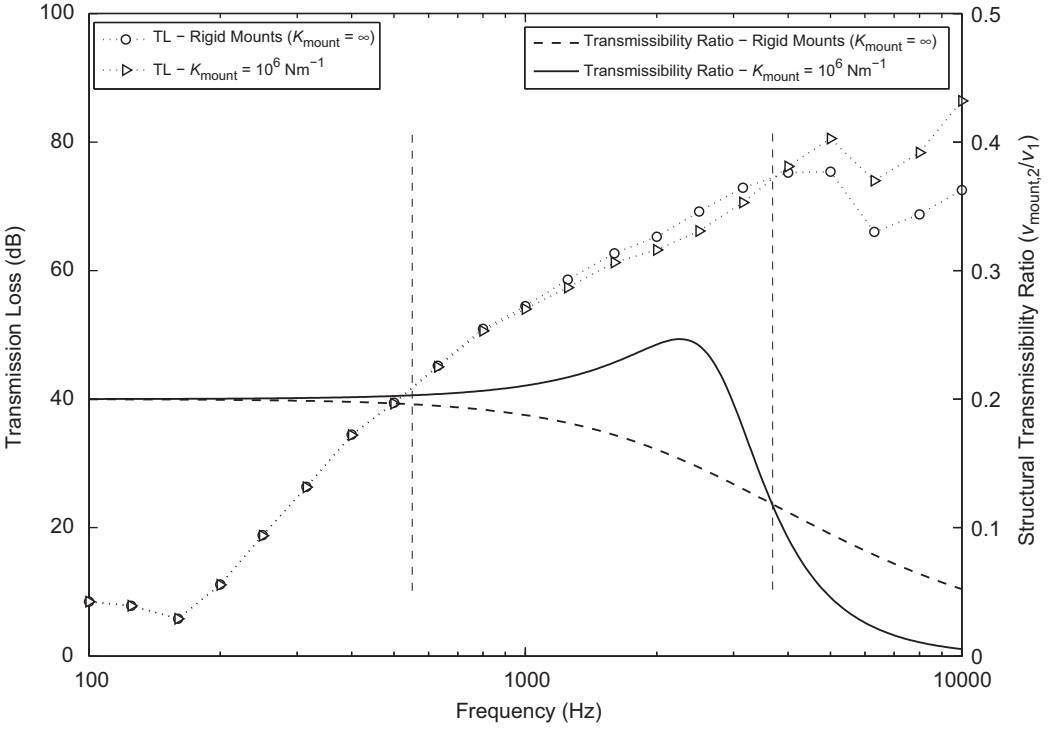

Fig. 4. Structural transmissibility vs. transmission loss.

For thin isotropic plates in bending, expressions for $Z_{p,1}$ and $Z_{p,2}$ are known ($Z_p = 8(Dm_s)^{1/2}$) [28] and thus the ratio $v_{mount,2}/v_1$ can be easily calculated for a quick assessment of the mounts effects using Eq (72). Actually, if the mounts' dynamics were described with a general four-pole formulation instead of a lumped mass-spring-mass system (see Eq. (54)), the following equation for the ratio $v_{mount,2}/v_1$ should be used:

$$\frac{v_{mount,2}}{v_1} = \frac{Z_{p,1}}{T_{12} + Z_{p,2}T_{11} + Z_{p,1}(Z_{p,2}T_{21} + T_{22})}. \tag{73}$$

However, for ribbed composite panels, simple expressions for $Z_{p,1}$ and $Z_{p,2}$ are not available and this is why the present model is relevant, i.e. to detect undesirable resonances between the mounts and complex structures. To assess the validity of the transmissibility analysis of the model, the ratio $v_{mount,2}/v_1$ was calculated for a simple double wall configuration made of un-ribbed isotropic aluminum panels. The panels' thicknesses were 1 mm (panel 1) and 2 mm (panel 2). Two values of mount stiffness were tested with this configuration: $K_{mount} = \infty$ (rigid mounts) and $K_{mount} = 10^6\,\mathrm{Nm}^{-1}$. The results for the two cases are presented in Fig. 4 together with the associated transmission loss. The rest of the parameters are the same as in the transmission loss calculations. Below 4 kHz, the ratio $v_{mount,2}/v_1$ predicts that the structural transmissibility with $K_{mount} = 10^6\,\mathrm{Nm}^{-1}$ will be higher than with rigid mounts due to a resonance. Therefore, the transmission loss should be lower for this case than with rigid mounts, which is exactly what is observed in Fig. 4. Above 4 kHz, the tendency is reversed and so is the transmission loss. The transition frequency between the two regimes is captured very well by the transmissibility analysis, which confirms its validity. This suggests that the latter analysis could be used to predict if a mount with known dynamic properties will create an undesirable resonance.

4.3. The influence of mount damping

Fig. 5 shows the effect of the mount damping for the composite configuration (results for the metallic configuration are not presented to avoid redundancy). Mount stiffness was kept constant ($K_{mount} = 10^6\,\mathrm{Nm}^{-1}$), but mount structural damping varied between 1 percent and 50 percent. The curves for rigid mounts and for airborne transmission only are also shown for comparison. As the damping of the mount increases, the TL increases in the region where the interaction of the mounts with the whole structure creates a resonance (between 200 and 315 Hz), but significant impacts are not seen elsewhere (less than 1 dB of difference). This indicates that having a sufficient level of structural damping for the mount is important to avoid deep TL dips in resonance regions (up to 5 dB of difference at 315 Hz between the curves for 1 percent and 50 percent of structural damping). This is consistent with the transmissibility analysis carried out in Section 4.2. It should be noted that similar conclusions were obtained with $K_{mount} = 10^7\,\mathrm{Nm}^{-1}$ between 4 and 10 kHz, but the results are not presented to avoid redundancy.

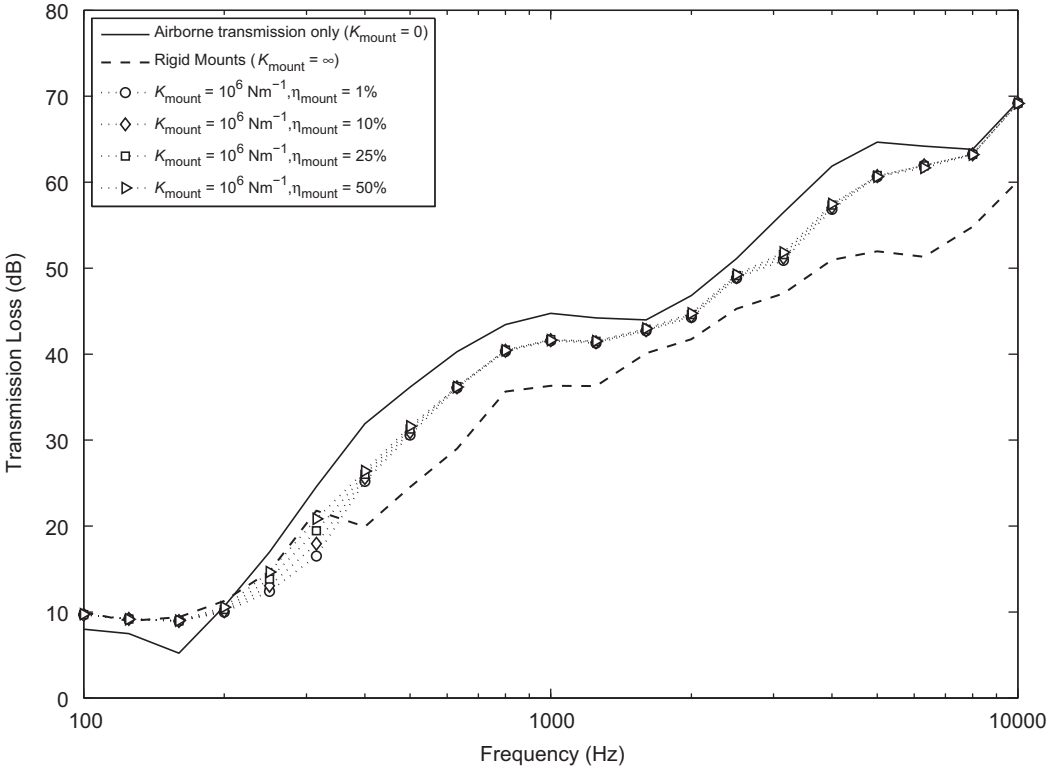

Fig. 5. The influence of mount damping (composite configuration).

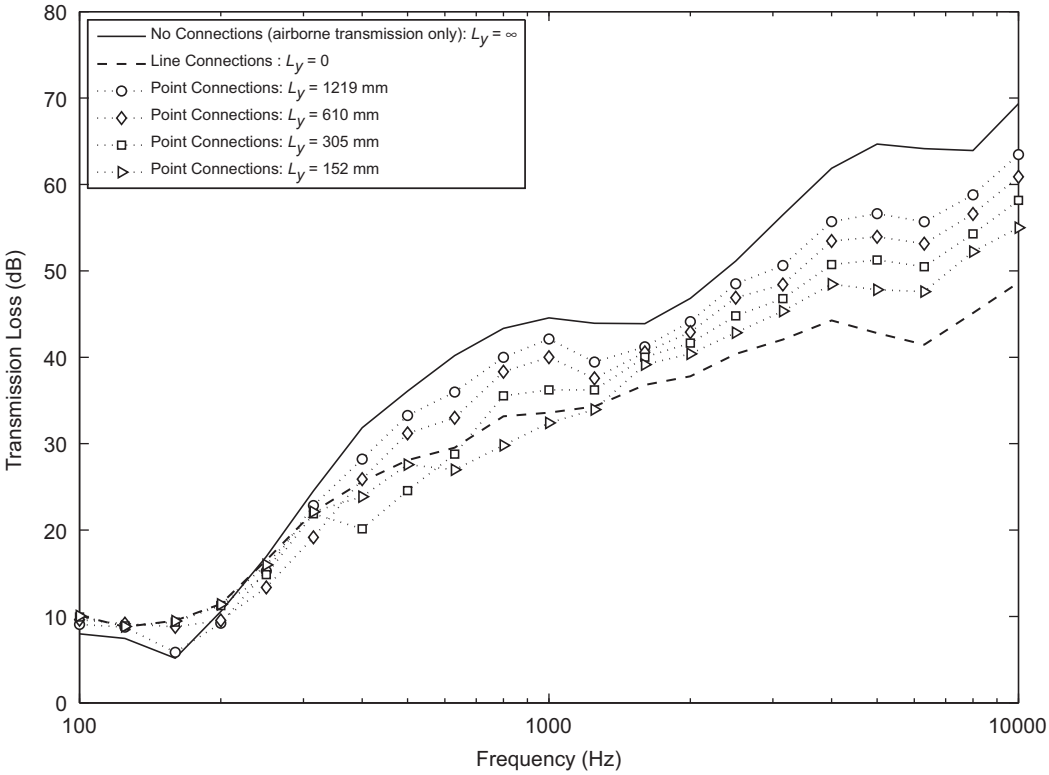

Fig. 6. The influence of mount spacing (composite configuration).

4.4. The influence of mount spacing

Fig. 6 illustrates the effects of mount spacing L_y for rigid ($K_{\text{mount}}=\infty$) and massless ($m_{\text{mount}}=0$) mounts. Six curves are compared in total: a curve where the mounts are absent ($L_y=\infty$), four curves where L_y takes values of 152 mm (6 in), 305 mm (12 in), 610 mm (24 in) and 1219 mm (48 in) and a final curve where a full line coupling condition is assumed between the ring frames and the panels ($L_y=0$). This last curve was obtained by adapting the model presented in Ref. [16] for the current study. To do so, the rotational coupling between the ring frames and the trim panel was suppressed in that model. Moreover, the number of terms q was adapted in function of L_y to ensure convergence (doubling $q_{\max}$ when L_y doubled was found to be adequate). As expected, when mount spacing decreases, more energy is transmitted from the skin to the trim and the TL is lowered. This is however not true for all frequencies since the TL with point connections is lower than the TL with a full line connection for a small range at mid-frequencies (the range is dependent on L_y). This behavior is attributable to the periodic nature of the structure (presence of pass-bands). The transition frequency at which the TL for point connections starts to be higher than the one for line connections is also in good agreement with the half bending wave length criteria mentioned in Section 2.2. For example, with $L_y=152$ mm, the transition frequency would be 1125 Hz ($=c_{\text{air}}/2L_y$), which is close to the observed value ($\sim$1250 Hz). Therefore, when rigid mounts are employed (which should be avoided), spacing must be set to the highest possible value in order to maximize the transmission loss.

4.5. The influence of cavity absorption

Fig. 7 presents the effect of cavity absorption on the transmission loss for mount stiffness and damping of $10^6\,\text{Nm}^{-1}$ and 1 percent. The absorption was modified by raising the flow resistivity σ_{fiber} of the fiberglass filling the cavity from 20 000 to 40 000 Nsm^{-4}. The other parameters in Table 2 were kept constant even though they are never totally independent from the flow resistivity in practice. Curves showing airborne transmission only ($K_{\text{mount}}=0$) for 20 000 and 40 000 Nsm^{-4} and a fifth curve showing structure-borne transmission only are also illustrated. Below 1 kHz, no observable effect occurs upon raising the absorption when the mounts are present and between 1 and 6.3 kHz, the effects remain limited (less than 1.5 dB of difference). In comparison, the increase in TL when the mounts are absent reaches almost 5 dB above 1 kHz. Such behavior is understandable since the structural path prevails over the airborne path at mid and high frequencies with a mount stiffness of $10^6\,\text{Nm}^{-1}$. Therefore, the principal effect of raising the absorption in the presence of mounts that do not fully inhibit structure-borne transmission is to add effective damping to the panels, which in the end does not reduce the

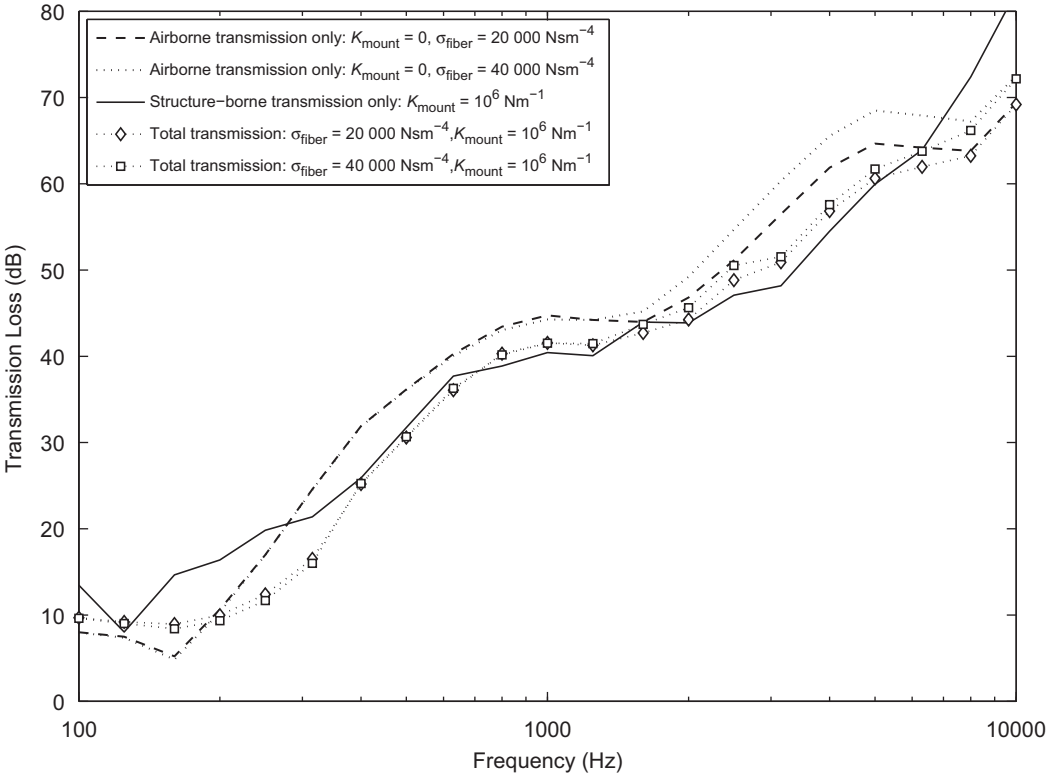

Fig. 7. The influence of cavity absorption (composite configuration).

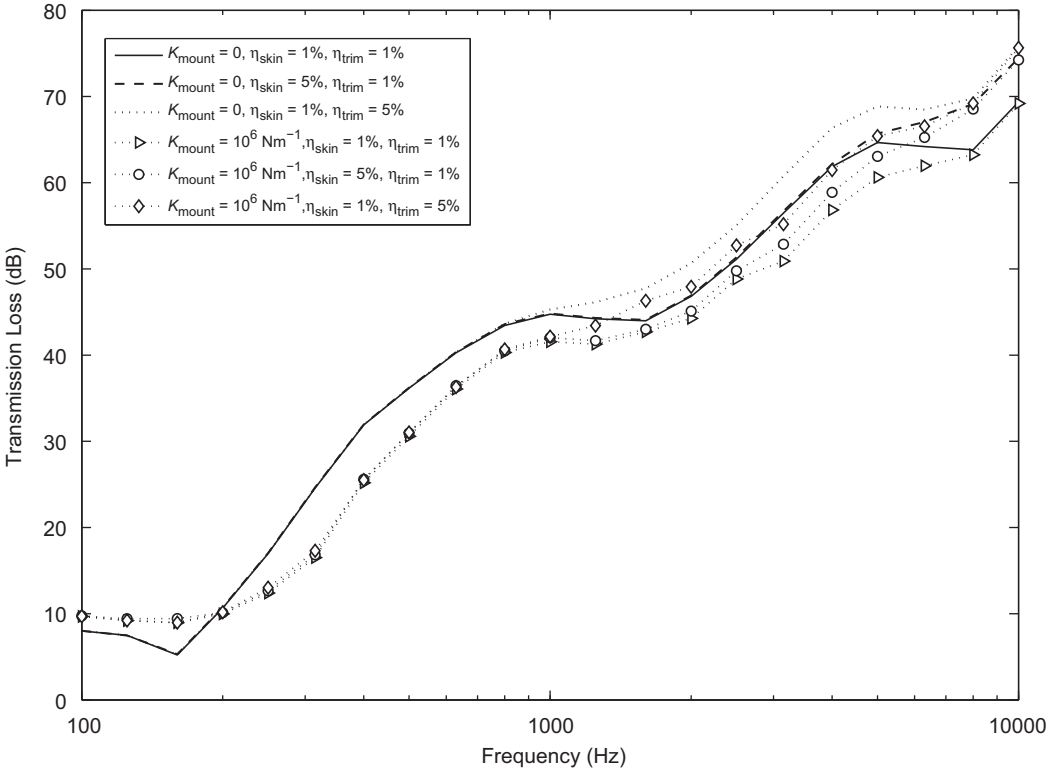

Fig. 8. The influence of panel damping (composite configuration).

whole transmission significantly. Above 6.3 kHz, the airborne transmission dominates again and the fiber becomes effective (the total transmission is almost equal to the airborne transmission).

4.6. The influence of panel damping

Fig. 8 compares the transmission loss for three configurations of skin panel and trim panel damping: η_{skin}=1 percent and η_{trim}=1 percent (original configuration), η_{skin}=5 percent and η_{trim}=1 percent, η_{skin}=1 percent and η_{trim}=5 percent. The selected 5 percent of damping represents a realistic and achievable level of damping. The modeling assumes however damping to be constant over the whole frequency range and does not account of any added mass (this is not the case in real life where damping is classically achieved using an attached damping layer). The comparison is done for the uncoupled configuration (K_{mount}=0) and a coupled configuration where the structure-borne and airborne transmission paths are of the same order of magnitude, (K_{mount}=10^6 Nm^{-1}; see Fig. 7). When the skin damping is raised to 5 percent, an increase in the transmission loss of 2–5 dB is observed for both the coupled and uncoupled configurations in the vicinity and above the critical frequency of the panel (above 5 kHz). Below this region, no significant effect occurs for the uncoupled configuration while an increase of 1–2 dB is seen for the coupled case starting around the critical region of the trim panel (1.6 kHz). These results confirm the experimentally known fact that above the critical frequency of the trim panel (1.6 kHz), if structure-borne transmission is present, the damping of the skin panel can make a difference, for diffuse field excitation, even below its critical frequency. Increases in the TL are also observed when trim damping is raised to 5 percent, except that this time, significant improvements in the TL begin at 1 kHz for both the coupled and uncoupled configurations. These improvements are, on average, more important compared to skin damping.

4.7. Comparison with finite elements

In order to validate the periodic model and to assess its limitations due to the assumption of an infinite structure, the latter was compared to finite element method—boundary element method (FEM-BEM) simulations for a full metallic structure made of a 2 mm thick aluminum panel (panel 1) and a 3 mm thick aluminum panel (panel 2). Attention was focused on the structure-borne path alone to see how well the periodic model reproduces the modal behavior associated to this path at low frequencies, but also to reduce the computational and memory usage cost of the FEM model by not meshing the fluid (a vacuum is assumed inside the cavity). Other parameters such as frame profile or frame and mount

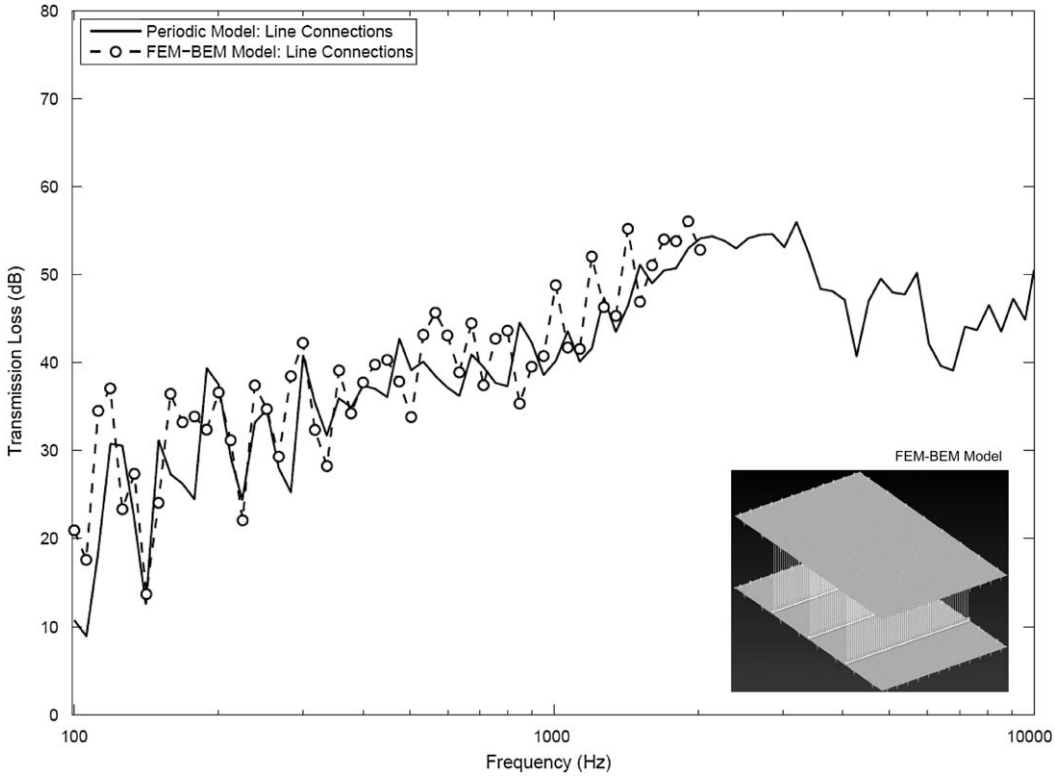

Fig. 9. Periodic Model vs. FEM—line connections.

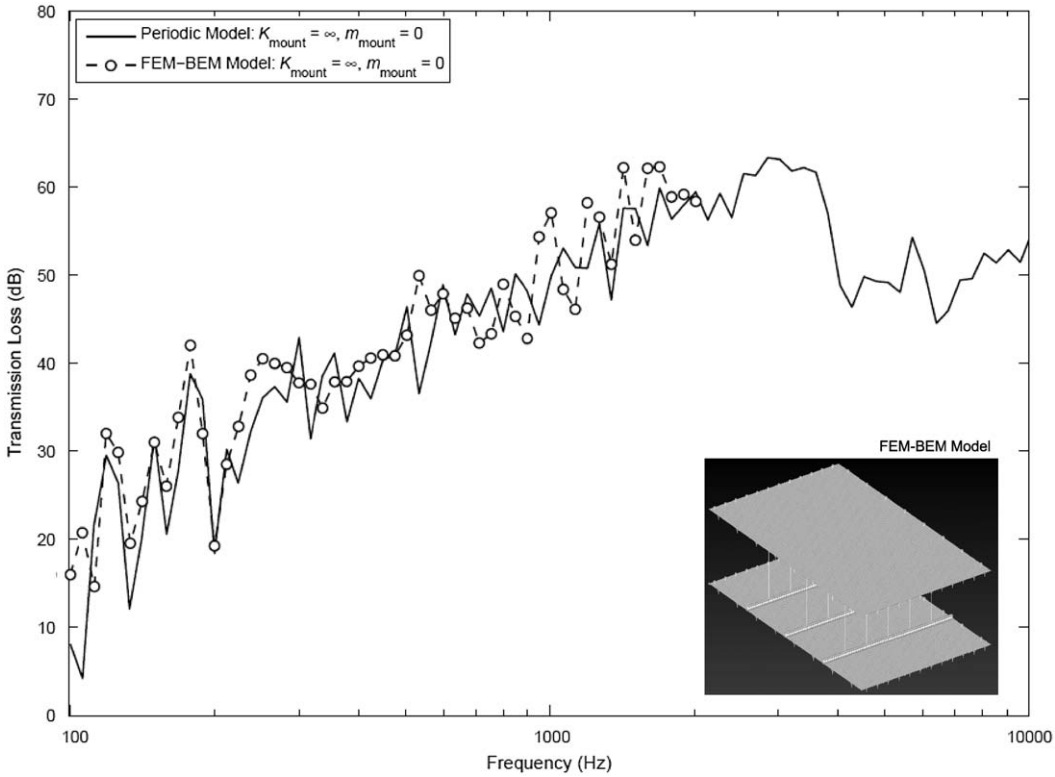

Fig. 10. Periodic Model vs. FEM—rigid and massless point connections.

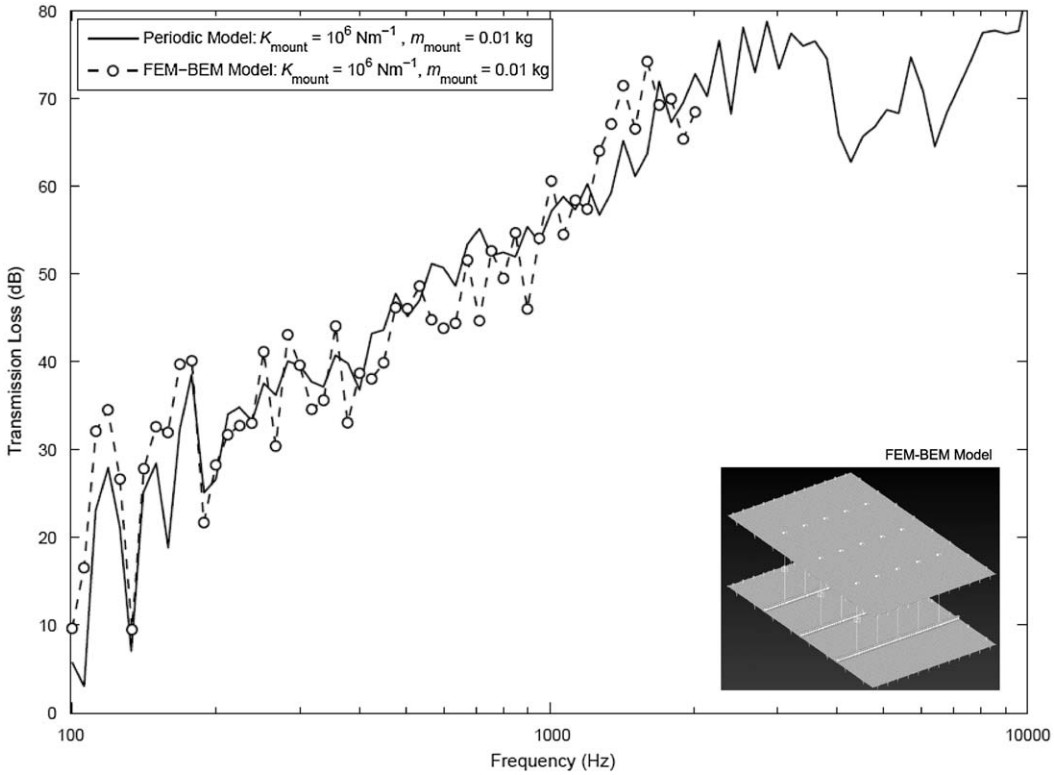

Fig. 11. Periodic Model vs. FEM—point connections with $K_{mount}=10^6\,Nm^{-1}$ and $m_{mount}=0.01\,kg$.

spacing (L_x=762 mm, L_y=305 mm) were kept constant. In the FEM model, the dimensions of the panels were 3042 mm along x and 1829 mm along y so that a total of 15 full periodic bays were contained within the boundaries. The panels were assumed to be simply supported along their edges. Calculations were made up to 2 kHz in 1/12 octave bands but the transmissibility was not averaged in 1/3 octave bands to avoid smoothing the modes. Modes ranging from 1 to 3 kHz were calculated with NASTRAN and an in-house boundary element solver was employed to calculate the TL using these modes (the code uses modal synthesis for the vibration response and Rayleigh's integral for the radiation response since the panels are assumed flat and baffled). A diffuse field approximated with a superposition of 64 planes waves (8 angles along the incident direction θ and 8 angles along the heading direction φ) was used. In total, 24 000 elements were used to mesh each panel (200 along x, 120 along y), so that the minimum criterion of 6 elements per unit wavelength was respected for all the modes of the 2 mm panel below 3 kHz. It should be noted that this structure is clearly not representative of aircrafts sidewalls and is only studied for validation purposes.

Three cases were tested and the results are presented in Figs. 9–11. The first case corresponds to a full line coupling between the two panels. As in the spacing study, the results for the periodic model were obtained by adapting the model presented in Ref. [16]. The second case corresponds to a discrete mount coupling in which L_y=305 mm, but where the mounts are assumed to be rigid and massless. Finally, in the third case, the mounts are also discrete (L_y=305 mm), but they are resilient with mass ($K_{mount}=10^6\,Nm^{-1}$; $m_{mount}=0.01\,kg$). Screenshots of the FEM-BEM geometry for these three cases are also given in the figures.

At first sight, the agreement between the periodic model and the FEM simulations is quite satisfying; the average level of transmitted energy is well reproduced at mid and high frequencies ($f>300$ Hz) for the three cases. However, the modes are not captured precisely with the periodic approach, especially at low frequencies. This was expected since the effects of finite dimensions and boundary conditions are more significant at low frequencies. Therefore, it is clear that by raising the panels' dimensions and incorporating more and more periodic bays into the FEM model, the agreement with the periodic model would increase and the frequency at which major discrepancies would be observed would get lower. Unfortunately, this cannot be done in practice due to calculations limitations. Still, the presented examples show a good agreement for the average level of transmitted energy, thus corroborating the validity of the presented model.

5. Conclusion

In this paper, an analytical model assessing the influence of trim mounts on the sound transmission of an aircraft sidewall representative double panel structure was presented. The effects of parameters that can be selected by designers

were studied and conclusions with practical impacts were drawn. First, it was seen that the use of resilient mounts could reduce the structure-borne transmission path significantly for both metallic and composite structures when they are properly designed (up to 20 dB of difference between rigid and resilient mounts). However, it was also observed that they could create undesirable resonances resulting from their interactions with the panels. To reduce the impact of these resonances, raising the structural damping of the mount was shown to be important. The effect of mount spacing was investigated for rigid mounts and the results confirmed that increased spacing means lower energy transmission (up to 25 dB of difference at mid and high frequencies when comparing the situation with no structural coupling to the one with a full line coupling). Therefore, if rigid mounts are employed—a choice that is not realistic for typical aircraft structures—a compromise must be made between acoustical insulation and structural constraints when selecting the spacing intervals. The study of cavity absorption showed that using a more efficient sound treatment package is not worth the investment if the structure-borne path is not adequately insulated and that the opposite situation was also true. This conclusion may seem intuitive and perhaps trivial, but the model could provide results in support of this statement. Moreover, the investigation of panel damping confirmed that in the presence of structure-borne transmission, raising the skin damping can increase the TL even below coincidence (from 1 to 2 dB of difference between 1 percent and 5 percent of damping below 5 kHz). However, in the vicinity and above the critical frequency of the trim panel, i.e. above 1 kHz, improvements are, on average, greater if trim damping is raised instead of skin damping. Finally, comparison between the periodic model and finite element simulations for structure-borne transmission show that the average level of transmitted energy is well reproduced with the periodic approach. However, the modes are only captured approximately due to the assumption of an infinite structure.

In conjunction with experimentally derived data for the four pole transmission parameters of the mounts in Eq. (54), the model could be used to provide a preliminary assessment of the performance of real mounts or conversely, to find what would be the ideal parameters for a given structure. Even so, it will be important in the future to continue adding refinement to it by including the panels' curvature, the presence of skin stringers, the handling of TBL excitation and the influence in plane tensions due to cabin pressurization. Ongoing work targeting the incorporation of these features will be presented in a future paper.

Appendix A. Calculation of the equivalent dynamic stiffness of the composite panel

When a wave of amplitude P is forced to propagate in the composite panel with a structural wavenumber $k_{\mathrm{str},pq}$ and a structural heading angle $\varphi_{\mathrm{str},pq}$, the equations of motion for the panel using Berthelot's flat laminate model [23] are

$$\begin{bmatrix} \beta_{11}-\rho_s\omega^2 & \beta_{12} & 0 & \beta_{14}-R\omega^2 & \beta_{15} \\ \beta_{21} & \beta_{22}-\rho_s\omega^2 & 0 & \beta_{24} & \beta_{25}-R\omega^2 \\ 0 & 0 & \beta_{33}-\rho_s\omega^2 & \beta_{34} & \beta_{35} \\ \beta_{41} & \beta_{42} & \beta_{43} & \beta_{44}-I_{xy}\omega^2+F_{55} & \beta_{45}+F_{45} \\ \beta_{51} & \beta_{52} & \beta_{53} & \beta_{54}+F_{45} & \beta_{55}-I_{xy}\omega^2+F_{44} \end{bmatrix} \begin{bmatrix} u_x \\ u_y \\ W \\ \phi_x \\ \phi_y \end{bmatrix} = \begin{bmatrix} 0 \\ 0 \\ P \\ 0 \\ 0 \end{bmatrix}, \tag{A.1}$$

where u_x and u_y represent the displacements of the panel's middle plane in the x and y directions, W its transverse displacement and ϕ_x and ϕ_y its angular displacements with the z axis in the xz and yz planes. The coefficients β_{ij} are

$$\beta_{11}=(A_{11}\cos^2\varphi_{\mathrm{str},pq}+2A_{16}\cos\varphi_{\mathrm{str},pq}\sin\varphi_{\mathrm{str},pq}+A_{66}\sin^2\varphi_{\mathrm{str},pq})k^2_{\mathrm{str},pq},$$

$$\beta_{12}=\beta_{21}=(A_{16}\cos^2\varphi_{\mathrm{str},pq}+(A_{12}+A_{66})\cos\varphi_{\mathrm{str},pq}\sin\varphi_{\mathrm{str},pq}+A_{26}\sin^2\varphi_{\mathrm{str},pq})k^2_{\mathrm{str},pq},$$

$$\beta_{14}=\beta_{41}=(B_{11}\cos^2\varphi_{\mathrm{str},pq}+2B_{16}\cos\varphi_{\mathrm{str},pq}\sin\varphi_{\mathrm{str},pq}+B_{66}\sin^2\varphi_{\mathrm{str},pq})k^2_{\mathrm{str},pq},$$

$$\beta_{15}=\beta_{51}=(B_{16}\cos^2\varphi_{\mathrm{str},pq}+(B_{12}+B_{66})\cos\varphi_{\mathrm{str},pq}\sin\varphi_{\mathrm{str},pq}+B_{26}\sin^2\varphi_{\mathrm{str},pq})k^2_{\mathrm{str},pq},$$

$$\beta_{22}=(A_{66}\cos^2\varphi_{\mathrm{str},pq}+2A_{26}\cos\varphi_{\mathrm{str},pq}\sin\varphi_{\mathrm{str},pq}+A_{22}\sin^2\varphi_{\mathrm{str},pq})k^2_{\mathrm{str},pq},$$

$$\beta_{24}=\beta_{42}=(B_{16}\cos^2\varphi_{\mathrm{str},pq}+(B_{12}+B_{66})\cos\varphi_{\mathrm{str},pq}\sin\varphi_{\mathrm{str},pq}+B_{26}\sin^2\varphi_{\mathrm{str},pq})k^2_{\mathrm{str},pq},$$

$$\beta_{25}=\beta_{52}=(B_{66}\cos^2\varphi_{\mathrm{str},pq}+2B_{26}\cos\varphi_{\mathrm{str},pq}\sin\varphi_{\mathrm{str},pq}+B_{22}\sin^2\varphi_{\mathrm{str},pq})k^2_{\mathrm{str},pq},$$

$$\beta_{33}=(F_{55}\cos^2\varphi_{\mathrm{str},pq}+2F_{45}\cos\varphi_{\mathrm{str},pq}\sin\varphi_{\mathrm{str},pq}+F_{44}\sin^2\varphi_{\mathrm{str},pq})k^2_{\mathrm{str},pq},$$

$$\beta_{34}=-\beta_{43}=\mathrm{j}k_{\mathrm{str},pq}(F_{55}\cos\varphi_{\mathrm{str},pq}+F_{45}\sin\varphi_{\mathrm{str},pq}),$$

$$\beta_{35}=-\beta_{53}=\mathrm{j}k_{\mathrm{str},pq}(F_{44}\cos\varphi_{\mathrm{str},pq}+F_{45}\sin\varphi_{\mathrm{str},pq}),$$

$$\beta_{44} = (D_{11}\cos^2\varphi_{\mathrm{str},pq} + 2D_{16}\cos\varphi_{\mathrm{str},pq}\sin\varphi_{\mathrm{str},pq} + D_{66}\sin^2\varphi_{\mathrm{str},pq})k^2_{\mathrm{str},pq},$$

$$\beta_{45} = \beta_{54} = (D_{16}\cos^2\varphi_{\mathrm{str},pq} + (D_{12}+D_{66})\cos\varphi_{\mathrm{str},pq}\sin\varphi_{\mathrm{str},pq} + D_{26}\sin^2\varphi_{\mathrm{str},pq})k^2_{\mathrm{str},pq},$$

$$\beta_{55} = (D_{66}\cos^2\varphi_{\mathrm{str},pq} + 2D_{26}\cos\varphi_{\mathrm{str},pq}\sin\varphi_{\mathrm{str},pq} + D_{22}\sin^2\varphi_{\mathrm{str},pq})k^2_{\mathrm{str},pq}. \quad (A.2)$$

The elastic constants A_{ij}, B_{ij}, D_{ij} and F_{ij} and inertial terms ρ_s, I_{xy}, and R are given by Berthelot [23]. By solving the matrix system in Eq. (A.1), the transverse displacement W is obtained and the dynamic stiffness of the panel associated with the wave propagating in the structure can be derived:

$$K_{\mathrm{panel},pq} = \frac{P}{W}. \quad (A.3)$$

It should be noted that the dispersion equations in Eq. (A.1) allow asymmetry of the composite panel even though a symmetric panel was considered for the skin in this study.

References

[1] L.R. Koval, Sound transmission into a laminated composite cylindrical shell, *Journal of Sound and Vibration* 71 (1980) 523–530.
[2] A. Blaise, C. Lesueur, On the sound transmission into an orthotropic infinite shell: comparison with Koval's results and understanding of phenomena, *Journal of Sound and Vibration* 150 (1991) 233–243.
[3] A. Blaise, C. Lesueur, Acoustic transmission through a 2-D orthotropic multi-layered infinite cylindrical shell, *Journal of Sound and Vibration* 155 (1992) 95–109.
[4] A. Blaise, C. Lesueur, Acoustic transmission through a "3-D" orthotropic multi-layered infinite cylindrical shell, *Journal of Sound and Vibration* 171 (1994) 651–664.
[5] K.H. Heron, Curved laminates and sandwich panels within predictive SEA, *Proceedings of the Second International AutoSEA Users Conference*, 2002.
[6] S. Ghinet, N. Atalla, H. Osman, The transmission loss of curved laminate and sandwich composite panels, *Journal of the Acoustical Society of America* 118 (2005) 774–790.
[7] S. Ghinet, N. Atalla, H. Osman, Diffuse field transmission into infinite sandwich composite and laminate composite cylinders, *Journal of Sound and Vibration* 289 (2006) 745–778.
[8] X.W. Yin, X.J. Gu, H.F. Cui, R.Y. Shen, Acoustic radiation from a laminated composite plate reinforced by doubly periodic parallel stiffeners, *Journal of Sound and Vibration* 306 (2007) 877–889.
[9] D.J. Mead, Y. Yaman, The harmonic response of rectangular sandwich plates with multiple stiffening: a flexural wave analysis, *Journal of Sound and Vibration* 145 (1991) 409–428.
[10] Y.F. Hwang, M. Kim, P.J. Zoccola, Acoustic radiation by point- or line-excited laminated plates, *ASME Journal of Vibration and Acoustics* 122 (2000) 189–195.
[11] T. Wang, V.S. Sokolinsky, S. Rajaram, S.R. Nutt, Assessment of sandwich models for the prediction of sound transmission loss in unidirectional sandwich panels, *Applied Acoustics* 66 (2005) 245–262.
[12] D.J. Mead, K.K. Pujara, Space-harmonic analysis of periodically supported beams: response to convected random loading, *Journal of Sound and Vibration* 14 (4) (1971) 525–541.
[13] J.-H. Lee, J. Kim, Sound transmission through periodically stiffened cylindrical shells, *Journal of Sound and Vibration* 251 (3) (2002) 431–456.
[14] C. Maury, P. Gardonio, S.J. Elliott, A wavenumber approach to modelling the response of a randomly excited panel, part I: general theory, *Journal of Sound and Vibration* 252 (1) (2002) 83–113.
[15] J. Brunskog, The influence of finite cavities on the sound insulation of double-plate structures, *Journal of the Acoustical Society of America* 117 (6) (2005) 3727–3739.
[16] J. Legault, N. Atalla, Numerical and experimental investigation of the effect of structural links on the sound transmission of a lightweight double panel structure, *Journal of Sound and Vibration* 324 (2009) 712–732.
[17] R.J.M. Craik, R. Wilson, Sound transmission through masonry cavity walls, *Journal of Sound and Vibration* 179 (1995) 79–96.
[18] R.J.M. Craik, R.S. Smith, Sound transmission through lightweight parallel plates. Part I: airborne sound, *Applied Acoustics* 61 (2000) 223–245.
[19] R.J.M. Craik, R.S. Smith, Sound transmission through lightweight parallel plates. Part II: Structure-borne sound, *Applied Acoustics* 61 (2000) 247–269.
[20] V. Cotoni, R.S. Langley, P.J. Shorter, A statistical energy analysis subsystem formulation using finite elements and periodic structure theory, *Journal of Sound and Vibration* 318 (2008) 1077–1108.
[21] J.F. Allard, *Propagation of Sound in Porous Media*, Elsevier Applied Science, London and New York, 1993.
[22] J.N. Reddy, *Mechanics of Laminated Composite Plates: Theory and Analysis*, CRC Press, Boca Raton, 1997.
[23] J.-M. Berthelot, *Matériaux Composites—Comportement mécanique et Analyse des structures*, Éditions TEC & DOC, Paris, 1999.
[24] B.R. Mace, Periodically stiffened fluid-loaded plates, I: response to convected harmonic pressure and free wave propagation, *Journal of Sound and Vibration* 73 (4) (1980) 473–486.
[25] D.J. Mead, Plates with regular stiffening in acoustic media: vibration and radiation, *Journal of the Acoustical Society of America* 88 (1990) 391–401.
[26] S. Timoshenko, D.H. Young, W. Weaver Jr., *Vibration Problems in Engineering*, Wiley, New York, 1974.
[27] J.N. Weisbeck, Key considerations for the successful specification and design of aircraft noise isolators, *Proceedings of the Internoise Conference*, Shanghai, China, 2008.
[28] F. Fahy, P. Gardonio, *Sound and Structural Vibration*, second ed, Academic Press/Elsevier, Oxford, UK, 2007.
[29] W.D. Pilkey, *Formulas for Stress, Strain and Structural Matrices*, second ed, Wiley, New York, 2005.
[30] J. Lee, S.-E. Kim, Free-vibration of thin walled composite beams with I-shaped cross sections, *Composite Structures* 55 (2002) 205–215.
[31] S. Ghinet S, N. Atalla, Vibro-acoustic behaviors of flat sandwich composite panels, *CSME Transactions* 30 (4) (2006) 473–493.
[32] S. Ghinet, N. Atalla, Noise transmission loss of orthotropic sandwich composite panels, Paper NC08-019, Noise-Con, 2008, Dearborn, MI, 28–30 July 2008.
[33] J. Wang, T.J. Lu, J. Woodhouse, R.S. Langley, J. Evans, Sound transmission through lightweight double-leaf partitions: theoretical modeling, *Journal of Sound and Vibration* 286 (2005) 817–847.